PIP$_2$ promotes conformation-specific dimerization of the EphA2 membrane region

Katherine M. Stefanski[1] , Charles M. Russell[2] , Justin M. Westerfield[2] , Rajan Lamichhane[2,*] , and Francisco N. Barrera[2,*]

From the [1]Graduate School of Genome Science and Technology, [2]Department of Biochemistry & Cellular and Molecular Biology, University of Tennessee, Knoxville, USA

Edited by Karen Fleming

The impact of the EphA2 receptor on cancer malignancy hinges on the two different ways it can be activated. EphA2 induces antioncogenic signaling after ligand binding, but ligand-independent activation of EphA2 is pro-oncogenic. It is believed that the transmembrane (TM) domain of EphA2 adopts two alternate conformations in the ligand-dependent and the ligand-independent states. However, it is poorly understood how the difference in TM helical crossing angles found in the two conformations impacts the activity and regulation of EphA2. We devised a method that uses hydrophobic matching to stabilize two conformations of a peptide comprising the EphA2 TM domain and a portion of the intracellular juxtamembrane (JM) segment. The two conformations exhibit different TM crossing angles, resembling the ligand-dependent and ligand-independent states. We developed a single-molecule technique using styrene maleic acid lipid particles to measure dimerization in membranes. We observed that the signaling lipid PIP$_2$ promotes TM dimerization, but only in the small crossing angle state, which we propose corresponds to the ligand-independent conformation. In this state the two TMs are almost parallel, and the positively charged JM segments are expected to be close to each other, causing electrostatic repulsion. The mechanism PIP$_2$ uses to promote dimerization might involve alleviating this repulsion due to its high density of negative charges. Our data reveal a conformational coupling between the TM and JM regions and suggest that PIP$_2$ might directly exert a regulatory effect on EphA2 activation in cells that is specific to the ligand-independent conformation of the receptor.

Eph receptor tyrosine kinases (RTKs) are the largest family of RTKs in humans. Eph receptors are involved in tissue patterning during embryonic development, neuronal plasticity, and wound healing (1, 2). Beyond their normal physiological functions, Eph receptors can contribute to human diseases. For example, elevated EphA4 signaling results in neuronal damage in Alzheimer's disease and amyotrophic lateral sclerosis (ALS) (3–6), and the loss of EphB2/B3 signaling is implicated in skeletal malformations that cause cleft palate (7). Moreover, a large body of research exists establishing that Eph receptors are overexpressed in a variety of cancer types. Specifically, EphA2 overexpression is found in breast, ovarian, prostate, and pancreatic cancers and is correlated with aggressive tumors, high rates of tumor recurrence, and poor patient prognosis (8–14). Additionally, Eph receptors have been found to be cellular receptors for viruses that cause cancer. For example, EphA2 is a receptor for Kaposi's sarcoma-associated herpes virus and Epstein–Barr virus (15, 16).

EphA2 signaling pathways control cell proliferation, migration, and cell retraction (17). EphA2 can engage in two modes of activation: ligand-dependent and ligand-independent (i.e., noncanonical). Ligand-dependent signaling requires activation of EphA2 by binding of its ligand, ephrinA1, resulting in the phosphorylation of residues Y588, Y594, and Y772. This results in signaling that inhibits metastatic phenotypes by causing cell retraction/rounding and decreasing cell proliferation and migration (1, 18, 19). Conversely, ligand-independent signaling is responsible for oncogenic phenotypes and occurs via phosphorylation of S897 by the kinases AKT, RSK, or PKA (18, 20–22). Overexpression of EphA2 in cancers is often accompanied by a loss of ephrinA1 ligands (23, 24). It is believed that this imbalance of EphA2 and ephrinA1 results in both increased ligand-independent signaling and a decreased ligand-dependent signaling, promoting tumor growth and malignancy (25).

Due to its prominent role in oncogenesis, EphA2 has become an attractive drug target and, as such, an active area of research. The structure of EphA2 includes an extracellular ligand-binding domain, a single-pass transmembrane domain (TMD), and an intracellular kinase domain connected to the TMD by a disordered juxtamembrane (JM) segment. In the ligand-unbound state, EphA2 exists in a monomer–dimer equilibrium (26). Upon binding of ephrinA1, EphA2 dimerization via the ligand-binding domains is promoted and leads to the formation of large signaling clusters (27). While some aspects of Eph receptor signaling have been elucidated, the exact molecular events of how the receptor transmits an extracellular signal across the plasma membrane remain unknown. As a membrane-spanning receptor, the TMD is expected to play a role in conferring signals across the plasma membrane.

PIP₂ is a specific ligand of the EphA2 receptor

An NMR structure of the EphA2 TMD dimer was solved by Bocharov *et al.* (28). This dimer had a small interhelical crossing angle (15°), and the interface was mediated by a heptad repeat (HR) motif. The same study conducted molecular dynamics (MD) simulations on the NMR structure and found that the EphA2 TMD dimer could rotate to a glycine zipper (GZ) interface with a larger interhelical crossing angle (45°). It was hypothesized that the receptor switches between these two conformations with different dimerization interfaces. In a follow-up study, it was reported that mutations in the HR motif decreased ligand-independent signaling, while mutations in the glycine zipper decreased ligand-dependent signaling (29). These findings, combined with the structural data, gave rise to the following model: In the ligand-independent active state, the EphA2 TMD dimerizes *via* the HR motif with nearly parallel TMDs, while in the ligand-dependent signaling state, EphA2 dimerizes *via* the GZ with tilted TMDs (28, 29). It is unknown how the switch in dimerization interface and opening of the interhelical crossing angle participate in conferring the extracellular signal from the outside of the cell to the cytoplasm. It is further unknown if the JM responds to changes in the TMD.

JM–lipid interactions are involved in the activation of several receptors. These interactions are believed to be mediated by positively charged JM residues interacting with negatively charged lipid head groups. For EphA2, associations between basic JM residues and phosphatidylinositol 4,5-bisphosphate (PIP₂) have been computationally predicted (30). Notably, the first five positively charged residues (HRRRK) of the EphA2 JM are predicted to establish strong interactions with negatively charged PIP₂. However, this association has not been experimentally observed. Interactions between the JM and PIP₂ might regulate the activity of EphA2, since the two signaling modalities of EphA2 alter PIP₂ levels. Ligand-dependent signaling activates PI3K, which phosphorylates PIP₂ to generate PIP₃ (1). While ligand-independent signaling recruits SHIP2, which converts PIP₃ to PIP₂ and can be triggered by AKT upon PI3K activation (17). However, it is unknown if these local changes in PIP₂ directly alter EphA2 signaling.

In the present study, we investigate how the TMD and JM regions of EphA2 are affected by signaling-related changes in TMD orientation and lipid environment. We use hydrophobic matching to stabilize the two conformations of the EphA2 TMD region. We also examine how bilayer composition and the position of JM residues affect self-assembly of the TMD of EphA2, using a novel single-molecule fluorescence approach in styrene maleic acid lipid particles (SMALPs). Our results indicate that PIP₂ specifically promotes dimerization of one of the two TMD conformations *via* interactions with the JM. Implications for the role of lipids in the two signaling states of EphA2 are discussed.

Results

Bilayer thickness drives changes in TM orientation

We sought to generate an *in vitro* model of the ligand-independent and ligand-dependent signaling states of the
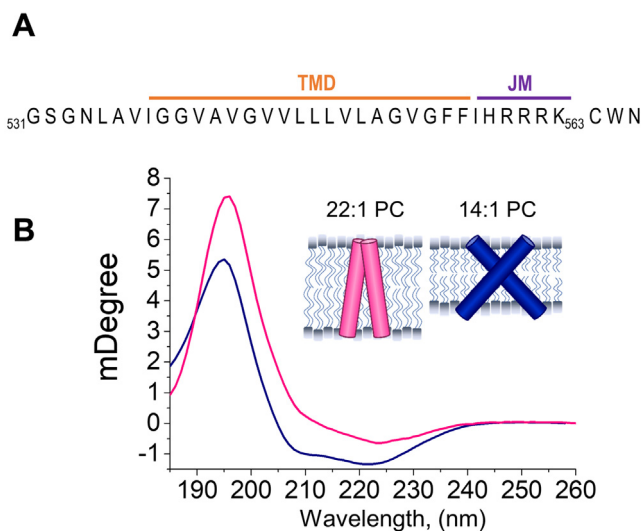

Figure 1. Bilayer thickness drives differences in TMJM helical tilt. *A*, sequence of the TMJM peptide comprised of EphA2 residues 531 to 563 with added CWN residues at the C terminus. *B*, OCD spectra of TMJM in 22:1 PC (fuchsia) and 14:1 PC (navy). *Inset*, model of the conformations of TMJM dimer in 14:1 PC and 22:1 based on OCD data.

membrane region of the EphA2. To this end, we used the TMJM peptide, which comprises a short stretch of extracellular residues, the TMD, and first five JM residues of EphA2 (Fig. 1*A*). At the C terminus, we added a cysteine to enable dye conjugation and a tryptophan as a fluorescent reporter of the JM segment. As noted above, the two EphA2 signaling configurations have different interhelical crossing angles. To promote the different configurations, we used model membranes composed of 14:1 PC or 22:1 PC, which only differ in the length of their acyl chains. Since 22:1 PC contains eight more tail carbons than 14:1 PC, it forms thicker bilayers (45.5 Å *versus* 29.6 Å) (31). Our hypothesis was that we could use hydrophobic matching to stabilize the TMD of EphA2 in the two different conformations (32). Specifically, TMJM would orient closer to the bilayer normal in a thick bilayer (22:1 PC), while it would tilt further away from the bilayer normal in a thin (14:1 PC) bilayer. Thus, we sought to use bilayer composition to tune helical tilt and recapitulate the ligand-independent and ligand-dependent signaling configurations.

We used oriented circular dichroism (OCD) to test the effects of bilayer thickness on the helical tilt of TMJM, when reconstituted in supported lipid bilayers composed of 14:1 PC or 22:1 PC. Figure 1*B* shows that the obtained OCD spectra had two α-helical minima at 208 and 224 nm, indicating a transmembrane orientation. To assess the helical tilt, we can examine changes in the 208 nm minimum. A more positive value indicates a less tilted helix, as seen in 22:1 PC, while a lower value indicates a more tilted helix, as seen in 14:1 PC (Fig. 1*B*) (33–35). These data suggest that, on average, the TMDs are more vertical in thicker bilayers, like the ligand-independent signaling configuration. In contrast, the TMDs are more tilted in thinner bilayers, which might correspond to the ligand-dependent signaling configuration. The observed
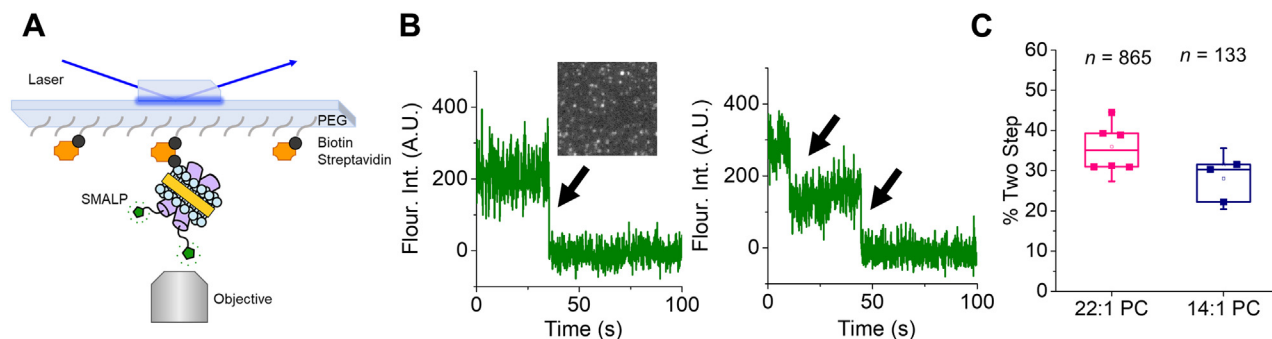
Figure 2. TMJM dimerization observed by single-molecule TIRF of SMALPs. *A*, schematic of TIRF experimental setup. SMALP showing SMA polymer (*yellow*) encircling lipids (*blue*) containing TMJM peptides (*purple*) labeled with Alexa Fluor 488 (*green*), immobilized on a PEGylated slide *via* a biotin (*black*) and streptavidin (*orange*) linkage. *B*, representative fluorescence traces showing one (left) and two (right) photobleaching steps (*black arrows*). Representative TIRF image of SMALPs (*inset*). *C*, box and whiskers plot (upper quartile, median, and lower quartile) showing percentages of peptide counted in traces with two photobleaching steps in 22:1 PC and 14:1 PC at a lipid-to-peptide ratio of 300:1. Data are from three to six independent experiments ±S.D, *n* is total number of traces counted with two photobleaching steps.

changes in tilt were independent of lipid-to-peptide ratio and were also observed at lower peptide concentrations (Fig. S1). Standard circular dichroism was performed on TMJM in 14:1 PC and 22:1 PC vesicles to ensure that the secondary structure of the peptide was similar in both lipids (Fig. S1). The OCD results suggest that the peptide responds to being placed in bilayers of different thickness by adjusting helical tilt, providing a means to further study the two observed conformations.

TMJM can form dimers in thin and thick bilayers

We wanted to investigate if TMJM self-assembled into biologically relevant dimers. To this end, we developed a single-molecule photobleaching method using SMALPs. TMJM labeled with the fluorescent dye Alexa Fluor 488 was purified by HPLC, and the purity assessed by MALDI-TOF, which showed that a single population corresponding to the conjugated peptide was used for experiments (Fig. S2). This labeled peptide was reconstituted in multilamellar vesicles (MLVs) composed of either 14:1 PC or 22:1 PC containing 3% biotinylated phosphatidylethanolamine (biotin-PE). The MLVs were then incubated with styrene maleic acid (SMA). SMA forms a polymer belt around units of lipid bilayer and proteins (Fig. 2A) (36, 37). Transmission electron microscopy (TEM) confirmed that lipid composition did not alter SMALP size (Fig. S3, A–B), and colocalization experiments confirmed SMALP composition (Fig. S4, A–E). SMALPs were immobilized on a microscope slide *via* a biotin–streptavidin linkage (Fig. 2A, Fig. S4) and imaging was conducted using total internal reflection fluorescence (TIRF) microscopy. By analyzing the fluorescence of individual SMALPs over time, we can count single fluorophores by detection of photobleaching events (Fig. 2B) to determine the number of labeled TMJM peptides contained in a single SMALP. We found a substantial fraction of the peptide existed in SMALPs yielding two photobleaching steps (Fig. 2C). The majority of SMALPs contained one or two labeled TMJM peptides. Only a small fraction of SMALPs had three or more photobleaching steps (Fig. S5, A–B). These results were robust as similar values were

found for two bleaching steps in 22:1 PC and 14:1 PC (Fig. 2C and Fig. S1). The single-molecule results suggest that TMJM is in a similar monomer–dimer equilibrium in 14:1 PC and 22:1 PC.

Helical tilt alters the environment of JM residues but not the distance from the bilayer surface

We next investigated if JM–lipid interactions are different in the two conformations adopted by TMJM. We also sought to understand if the change in helical tilt observed for TMJM in thin and thick bilayers altered the position of the JM residues. We used the tryptophan placed after the JM residues as a reporter (Fig. 1A), and fluorescence experiments were performed in 14:1 PC and 22:1 PC vesicles (Fig. S9A). We observed that the fluorescence intensity of the tryptophan was higher in 14:1 PC than 22:1 PC (Fig. 3A) but the spectral maximum was similar (Fig. S6C). These data suggest a small change in the environment of the tryptophan that is not related to differences in membrane burial of the JM but may be due to differences in relative orientation (38).

We next examined the association of the JM with the bilayer interface using the tryptophan as a FRET (Förster Resonance Energy Transfer) donor and a headgroup-labeled dansyl phosphatidylethanolamine (DNS-PE) as an acceptor. In both 14:1 PC and 22:1 PC liposomes, a decrease in donor fluorescence was observed upon the addition of 0.25 to 3% acceptor, indicating that FRET occurred in all conditions (Fig. S7A). By calculating the FRET efficiency (E) at 0.5% acceptor we were able to quantify that the FRET occurring in 22:1 PC and 14:1 PC was similar (Fig. 3B). These data, combined with the tryptophan fluorescence results (Fig. 3A), led us to conclude that helical tilt alone does not significantly affect the association of the JM residues of TMJM with PC lipid bilayers.

PIP$_2$ drives changes in JM–headgroup distance only in thick membranes

To begin examining the effects anionic lipids have on the TMD orientation and JM–lipid associations, we repeated the OCD experiments in the presence of 3% PIP$_2$. We observed no
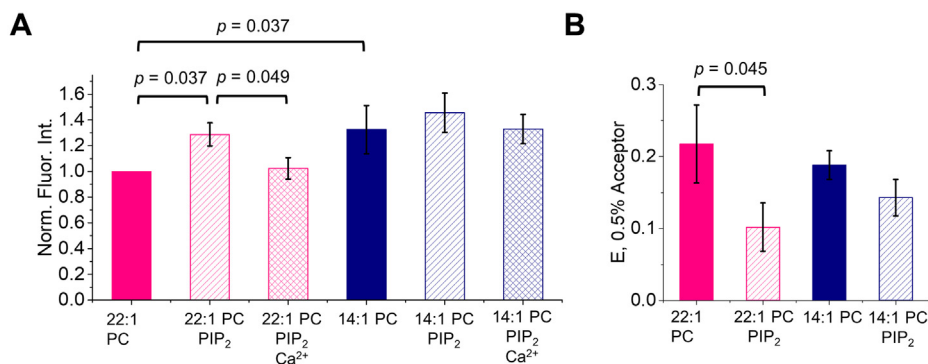
Figure 3. Bilayer thickness and PIP$_2$ alter Trp environment while PIP$_2$ changes headgroup distance. *A*, normalized intensities (350 nm) of TMJM Trp in 22:1 PC and 14:1 PC liposomes in the presence and absence of PIP$_2$ and 5 mM Ca^{2+}. *p*-values were determined by Mann–Whitney *U* tests, bars are means ± S.D., *n* = 3. *B*, FRET efficiencies calculated from FRET experiments with TMJM (Trp, donor) in 14:1 PC and 22:1 PC liposomes in the presence and absence of 3% PIP$_2$ (0.5% DNS-PE, acceptor) in liposomes. Bars are means ± S.D., *n* = 3. *p*-value is from one-way ANOVA followed by Tukey post-hoc test.

large shifts in helical tilt caused by the addition of PIP$_2$ in either thin or thick bilayers (Fig. S8, *A–B*). Therefore, we conclude that the addition of anionic lipids does not perturb the hydrophobic matching-driven changes in helical tilt observed in the original OCD experiments (Fig. 1*B*)

We next determined if PIP$_2$ could cause changes in JM–membrane interactions. We performed both tryptophan fluorescence and FRET measurements. When examining tryptophan fluorescence, we added the divalent cation Ca^{2+} as a control to shield the negative charges on PIP$_2$. Saturating levels of Ca^{2+} were used in these experiments as determined by calcium influx assays (Fig. S9*B*). In 22:1 PC, we observed a statistically significant increase in tryptophan fluorescence in the presence of PIP$_2$ (Fig. 3*A*). The observed intensity increase was reversed upon the addition of Ca^{2+} (Fig. 3*A*). This result suggests that cationic JM residues participate in electrostatic interactions with the anionic PIP$_2$ headgroups and that this interaction is placing the JM tryptophan into a different position. However, there were no significant fluorescence intensity changes in 14:1 PC in the presence of PIP$_2$, suggesting that in a more tilted TM configuration, the JM residues are less sensitive to electrostatic interactions with PIP$_2$ (Fig. 3*A*). There were no significant spectral maxima changes for either 14:1 PC or 22:1 PC upon the addition of PIP$_2$ (Fig. S6*C*).

When we performed FRET experiments to determine the effect of PIP$_2$ on the JM region, we observed differences in FRET efficiency across a range of acceptor concentrations, as before (Fig. S7*C*). Figure 3*B* shows that in thick bilayers, the presence of PIP$_2$ decreased FRET by roughly half. This result reasonably suggests that PIP$_2$ increases the distance between the JM tryptophan and the DNS-labeled lipid headgroups. By contrast, in thin bilayers, PIP$_2$ induced no significant changes in FRET efficiency (Fig. 3*B*). These results agree with the Trp fluorescence intensity changes caused by PIP$_2$ observed in thick bilayers (Fig. 3*A*).

PIP$_2$ drives increased oligomerization of TMJM only in thick membranes

Since changes in oligomerization accompany changes in EphA2 signaling in cells (26, 39), we next determined if the interactions observed between the JM residues and PIP$_2$ influenced the oligomerization of the peptide. Specifically, we used the single-molecule TIRF approach to examine the effect of PIP$_2$ on the self-assembly of TMJM, in thin and thick SMALPs. We determined *via* TEM that the addition PIP$_2$ did not alter SMALP size (Fig. S3). The data in Figure 4*A* show that PIP$_2$ increased the percentage of SMALPs with two photobleaching steps, suggesting an increase in the amount of dimeric TMJM peptide in 22:1 PC. The increased dimerization was reversed in the presence of Ca^{2+}, indicating that this effect is due to an electrostatic interaction between the polybasic JM and the anionic PIP$_2$ headgroup. While Ca^{2+} can destabilize SMALPs, this effect is observed only at higher concentrations (>2 mM) than we employed (40). In contrast, PIP$_2$ did not affect dimerization in 14:1 PC (Fig. 4*B*), nor do the counts for larger oligomers demonstrate sensitivity to PIP$_2$ (Fig. S5, *A–B*). These data agree with the tryptophan fluorescence and FRET data, which indicate that TMJM is sensitive to PIP$_2$ only in thick bilayers. Our data suggest that PIP$_2$ has a specific effect, which is limited to the conformation TMJM adopts in thick bilayers. Further, this effect is likely due to JM–PIP$_2$ electrostatic interactions.

To further investigate the effects of JM interactions on the self-assembly of TMJM, we performed SDS-PAGE experiments where dimerization was investigated by disulfide cross-linking. We reasoned that if PIP$_2$-dependent changes in self-assembly are promoted by lipid–JM interactions, this effect would be observable as differences in band sizes on a protein gel. Instead of measuring TMD–TMD interactions, as in the single-molecule experiments, we instead examined JM–JM interactions. To do this, TMJM containing a free Cys residue at the JM end was reconstituted in liposomes of 14:1 PC and 22:1 PC in the presence and absence of 3% PIP$_2$. The peptide stock, resuspended in buffer with SDS and loaded without DTT, remained monomeric (Fig. 4*C*, first lane). In the absence of a reducing agent, we observed two bands corresponding to monomer and disulfide-mediated dimer in all lipid conditions (Fig. 4*C*). The relative percentage of monomer and dimer was determined for each lipid condition. We observed that in 22:1 PC + PIP$_2$ vesicles, the percentage of the disulfide-mediated
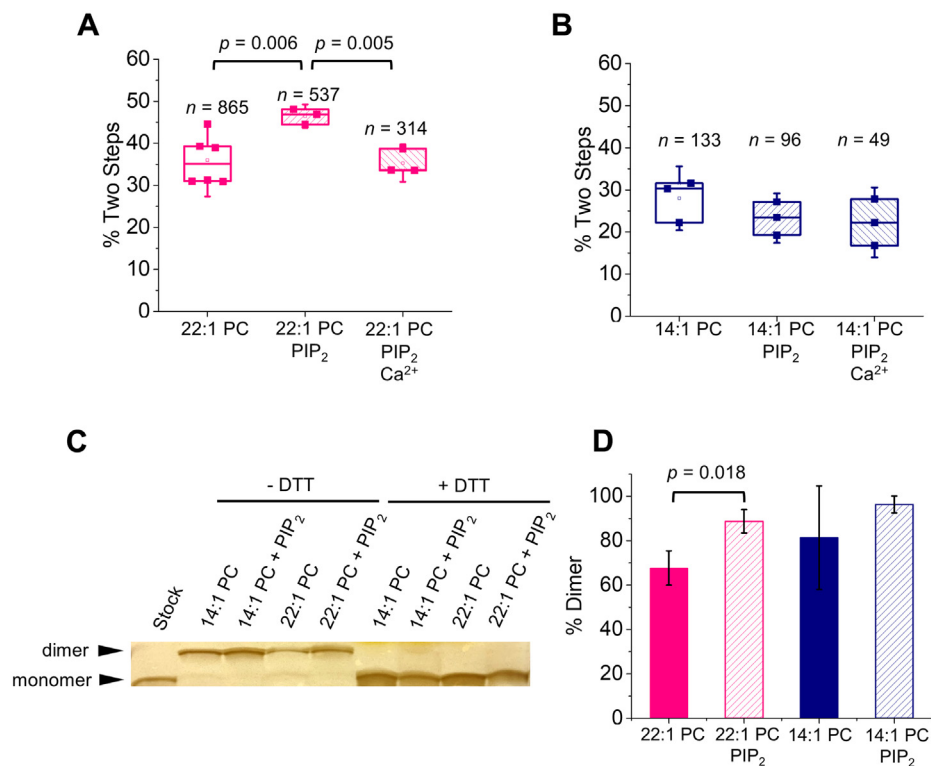
Figure 4. PIP₂ promotes self-assembly of TMJM in thick bilayers. *A–B*, percentage of Alexa Fluor 488 labeled TMJM peptide in two-step photobleaching traces in 22:1 PC and 14:1 SMALPs, respectively, determined by single-molecule studies. The effect of the presence of 3% PIP₂ and 1 mM Ca²⁺ is investigated. Data are from three to six independent experiments. *n* is number traces counted for each. *p*-values are from Student's *t*-tests with significance determined after Benjamini–Hochberg procedure. *C*, representative SDS-PAGE (full gel can be seen in Fig. S10) of unlabeled TMJM in 14:1 PC and 22:1 PC liposomes in the presence and absence of 3% PIP₂. Monomer and disulfide-mediated dimers can be seen in nonreducing conditions. Addition of 5 mM DTT eliminates the disulfide-mediated dimer band. *D*, quantification of three independent SDS-PAGE experiments as shown in *C*. Bands in each lane were quantified in ImageJ and percent of dimer was calculated. Bars are means ± S.D., *p*-value is from a Student's *t*-test. All data are from experiments at a lipid-to-peptide ratio of 300:1.

dimer was higher than in 22:1 PC alone (Fig. 4*D*), in agreement with the single-molecule data in SMALPs. In 14:1 PC, no effect of PIP₂ was observed.

PS alters JM environment but not dimerization in thick membranes

Given the effects of PIP₂ on TMJM, we wondered if phosphatidylserine (PS), an anionic lipid abundant at the plasma membrane, would also exert similar effects on the JM residues and dimerization of TMJM. The net charge of PS is −1, while PIP₂ has on average a charge of ∼−3 (41). To achieve a similar net charge in our model membranes, we used 22:1 PC with 10% PS (compared with 3% PIP₂). This value is similar to PS levels found in the plasma membrane of eukaryotic cells (42). We tested for changes in tryptophan fluorescence and oligomerization in 22:1 PC, where PIP₂-dependent changes were observed previously. A significant increase in fluorescence intensity was observed in the presence of PS (Fig. 5*A*). However, unlike the PIP₂ experiments, this increase was not fully reversed in the presence of saturating amounts of Ca²⁺, suggesting differences in the effect of the two anionic lipids. Furthermore, single-molecule experiments showed that the presence of PS did not promote dimerization (Fig. 5*B*). These data suggest that PS alters the environment of the JM residues

like PIP₂, but without simultaneously driving significant changes in dimerization.

Discussion

We have developed a reconstitution system that stabilizes the membrane region of the EphA2 receptor in two different conformations. OCD experiments performed in 14:1 PC bilayers indicated that the TMJM peptide adopted a highly tilted TM orientation (Fig. 1*B*), while in 22:1 PC bilayers the α-helix aligns more perpendicular to the bilayer plane (43). It is theoretically possible to use OCD to calculate specific helical tilt angles (44), but we could not accurately carry out this approximation due to uncertainties in peptide density in the supported bilayers employed. However, there is an intriguing qualitative agreement between our data and the two TM conformations reported for EphA2 (28, 29). The ligand-dependent dimer crosses the membrane in a highly tilted state (45°), while the ligand-independent dimer has a small crossing angle (15°) (28, 29). We propose that the two conformations found in our experimental conditions might correspond to the structure of the membrane region of EphA2 in the two different activation states: in 22:1 PC dimerization would occur with almost parallel helices, as expected for the ligand-independent dimer, and in 14:1 PC, a high-crossing
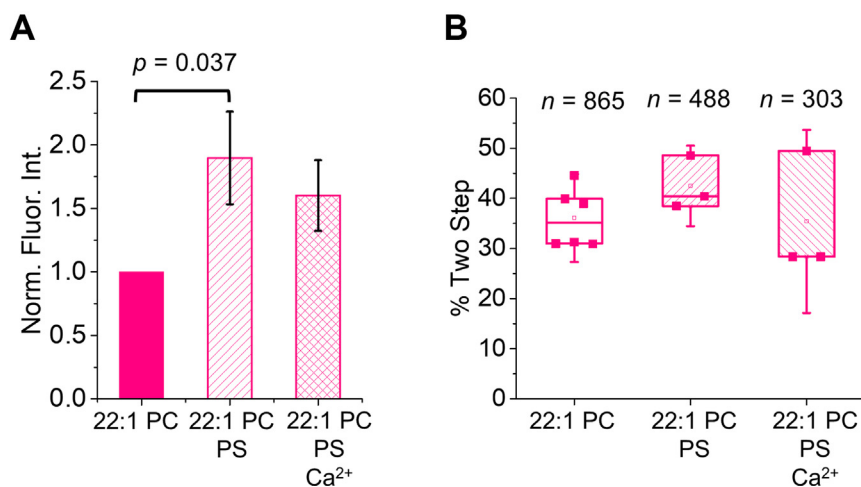
Figure 5. PS interactions with TMJM in thick bilayers. *A*, normalized fluorescence intensities from emission spectra of TMJM in 22:1 PC liposomes with 10% POPS and 5 mM Ca^{2+}. Bars are means ± SD, $n = 3$. *p*-value was determined by Mann–Whitney *U* test. *B*, percentages of dimeric TMJM from SM-photobleaching experiments in 22:1 PC examining effects of 10% POPS and 1 mM Ca^{2+}. Data are from three to six independent experiments. *n* is number traces counted for each. No statistically significant differences were found.

angle dimer would correspond to the conformation induced after ephrinA1 binding. Our data indicate that conformational selection can be accomplished using thin and thick bilayers by taking advantage of the strong propensity of TMDs to avoid hydrophobic mismatch (32). It is worth noting that it is possible that TMJM is randomly oriented in the OCD samples and that JM residues could have up/down orientation relative to the plane of the bilayer. However, since the lipids we examined are expected to be symmetrically distributed across the two monolayers, the lipid environment experienced by TMJM is expected to be equivalent regardless of TMJM orientation.

To ensure that the TMJM engages in biologically relevant dimerization, we employed two complementary methods. After finding artifacts in ensemble FRET experiments performed in liposomes, we endeavored to develop a new single-molecule approach that uses SMALPs, which have been shown to maintain native membrane structures (Fig. 2) (36, 37). We used the percentage of SMALPs displaying two photobleaching steps as a proxy for TMJM dimerization, but we cannot rule out that we are overestimating the number of dimers due to SMALPs capturing noninteracting monomers. We also performed a cross-linking assay in vesicles of the same lipid compositions as the SMALPs. While this second method does not measure dimerization *per se*, it is expected to report on a related event, the proximity of the JM cysteines. With this limitation in mind, it is possible that the methods do not give an exact measurement of the amount of dimer in equilibrium, but an adequate estimation to make comparisons between different lipid environments. Not surprisingly, the two methods yielded different levels of total dimerization of TMJM. However, they agree in reporting comparable levels of the dimer found in both 14:1 PC and 22:1 PC (compare Figs. 2*C* and 4, *C–D*). We conclude from the dimerization and OCD data that our thin and thick bilayer systems promote two different helical orientations of TMJM and that in both cases the peptide can form a dimer.

The JM segment of EphA2 is functionally important, as it contains residues Y588 and Y594, which can be phosphorylated by the kinase domain of EphA2. This event triggers the release of the receptor from the autoinhibited state (17). Hedger *et al.* (30) examined the interaction of basic JM residues of 58 RTKs with anionic lipid headgroups *via* MD studies. They concluded that JM residues closest to the TM establish significant contacts with PIP_2. Specifically for EphA2, their simulations predicted that the HRRRK region of the JM contributed the most to contacts with PIP_2. Based on this observation, we included the HRRRK residues in the TMJM peptide. Similar observations have been made in simulations of the JM and kinase domain of EphA2 in bilayers containing PIP_2 (45). However, these JM–PIP_2 interactions have never been experimentally demonstrated.

Using the tryptophan near the C terminus as a sensor, we were able to assess the JM environment in different lipids. Typically, the burial of tryptophan in a membrane results in a blue shift of the spectral maximum and a concurrent increase in fluorescence intensity (38). The change in bilayer thickness significantly affected the tryptophan fluorescence intensity, but no accompanying shift in spectral maximum was observed. This uncoupling of intensity and spectral maximum could be due to adjacent residues that quench tryptophan fluorescence. Specifically, the neighboring cysteine residue can engage in excited-state electron transfer with tryptophans (46). Further, it has been shown that tryptophan fluorescence spectra are sensitive to nearby charged residues (47). This led us to conclude that the local environment of the tryptophan is different in thin and thick bilayers, not because of differences in membrane burial but due to changes in relative orientation or proximity to neighboring residues. When PIP_2 was added to thick bilayers, the tryptophan fluorescence increased significantly and was reversed upon the addition of Ca^{2+}. This observation indicates that an electrostatic interaction occurs between the polybasic JM residues and the anionic PIP_2 headgroups. We did not observe fluorescence changes with
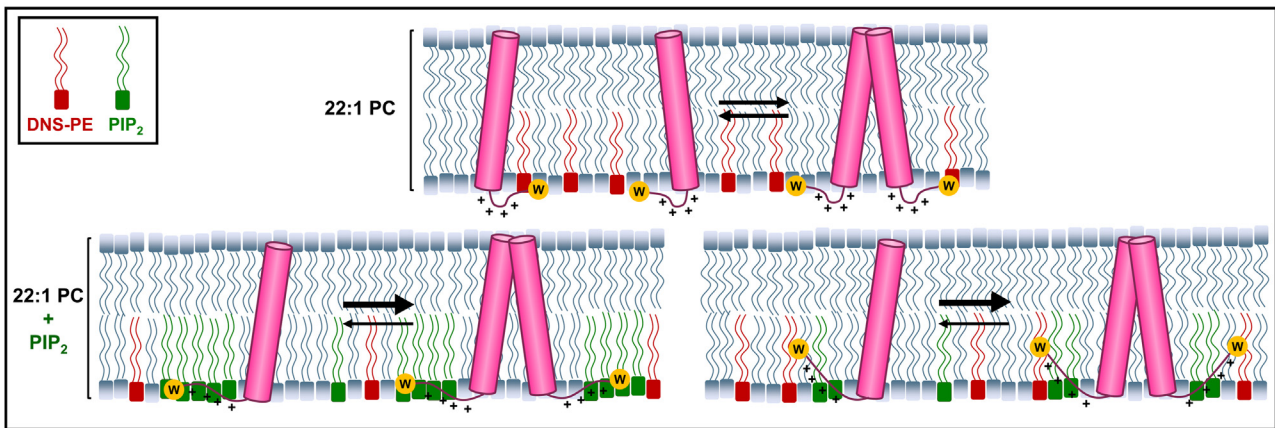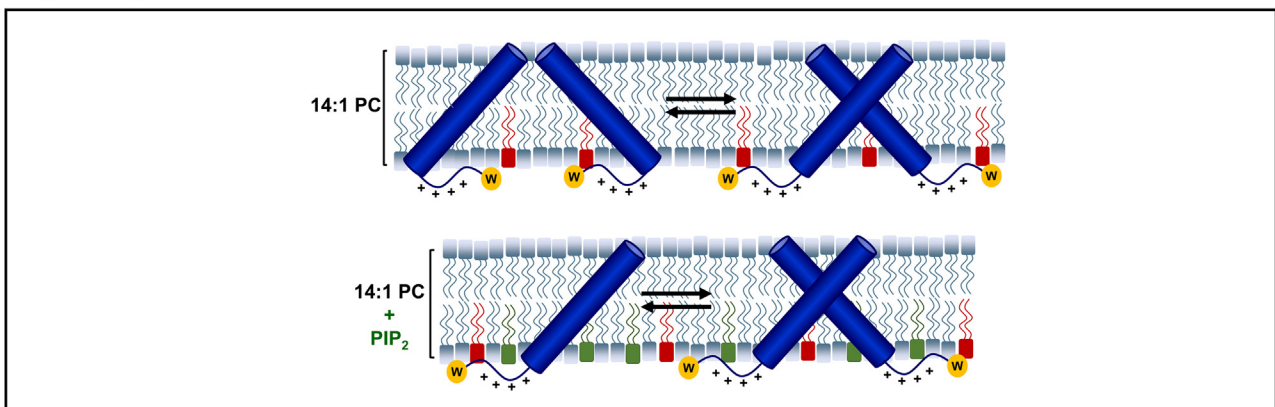
Figure 6. Model TMJM showing different effect of PIP$_2$ on two TMJM configurations. *Top*, in the ligand-independent signaling configuration TMJM exists in a monomer–dimer equilibrium in the absence of PIP$_2$. Charge–charge repulsion of the JMs must be overcome for efficient dimerization. In the presence of PIP$_2$ the JM–lipid association changes by either clustering of PIP$_2$ around the JM or burial of the JM. This shields the positive charges promoting dimerization. *Bottom*, in the ligand-independent signaling configuration, due to the tilt of the TM, charge repulsion of the JMs is not present. Neither JM environment nor dimerization is altered by PIP$_2$.

PIP$_2$ in thin bilayers, indicating that the peptide is not sensitive to the charged lipids in this alternate conformation. To explain the increase in tryptophan fluorescence intensity and the decrease in FRET observed only in 22:1 PC membranes in the presence of PIP$_2$, we have developed two possible explanations (Fig. 6). First, it is possible that the JM becomes more buried into the core of the membrane moving the Trp away from the headgroups. Alternatively, PIP$_2$ may cluster around the JM residues and this crowding pushes the DNS-PE headgroups away from the tryptophan laterally in the plane of the bilayer. We consider that these are the most plausible explanations for the observed experimental changes, but we cannot rule out other alternatives.

In single-molecule experiments, PIP$_2$ promoted TMJM dimerization in thick bilayers. Disulfide cross-linking experiments supported that PIP$_2$ promotes self-assembly in 22:1 PC bilayers. In thin bilayers, no PIP$_2$-dependent changes in disulfide-mediated dimerization were observed, also in agreement with the single-molecule data. Based on previous work (28, 29) and our data, we propose a model in which the EphA2 TMD and JM could synergize. In the ligand-independent state, EphA2 dimerization is mediated by the

heptad repeat motif resulting in an upright TM orientation. In this configuration, the JM residues are tightly associated with the inner leaflet of the cell membrane *via* electrostatic interactions with PIP$_2$. This interaction prevents electrostatic repulsion of the JM segments to make dimerization more energetically favorable. (Fig. 6, top). Without PIP$_2$, EphA2 dimerization would be less favorable due to the charge–charge repulsion of the JMs. Taken together, our results suggest that interaction of PIP$_2$ with the JM segments promotes TMD–TMD dimerization only when helices are roughly parallel.

On the other hand, in the ligand-dependent state, the TMD dimers would rotate to the glycine zipper dimerization interface and open to create a larger interhelical crossing angle. With the larger crossing angle of the dimer, charge–charge repulsion due to the JMs is minimized, and thus PIP$_2$ would not promote dimerization. A relief of charge repulsion during ligand binding has been observed for the growth hormone receptor, where extracellular JM residues engage in charge–charge repulsion, which is overcome by ligand binding and allows the TMD dimer to rotate and open to a larger interhelical crossing angle (48).

PIP₂ is a specific ligand of the EphA2 receptor

Tryptophan fluorescence data with PS suggest that, as with PIP$_2$, electrostatic interactions are enough to alter the environment of the JM region. However, unlike PIP$_2$, the interaction with PS is not fully reversed upon addition of saturating amounts of Ca^{2+}. This could be due to differences in binding sites and stoichiometry of the two lipids with Ca^{2+} ions (49, 50). Interestingly, PS did not promote dimerization, and the tryptophan fluorescence changes were larger. This leads us to conclude that JM interactions with PS do alter the environment of the JM but without promoting dimerization. In this case, the charge density of PS may not be large enough to overcome the charge–charge repulsion caused by the JM polybasic stretch. It has been reported that PS engages in contacts with RTK JM residues to a lesser degree than PIP$_2$, which may explain why we see an uncoupling of the effect of PS on JM environment and oligomerization (30).

Our biophysical data suggest that PIP$_2$ might play a direct role in modulating EphA2 signaling by stabilizing ligand-independent dimers and holding the phosphorylatable JM tyrosine residues at the plasma membrane. One study proposed that the ligand-independent oncogenic signaling is caused primarily by monomeric EphA2 (26). By promoting dimerization of the ligand-independent conformation, PIP$_2$ would be reducing oncogenic signaling. However, dimerization *via* PIP$_2$ in the unliganded state can be potentially opposed by the SAM domains, which are known to inhibit oligomerization (51). PIP$_2$–JM interactions have been demonstrated experimentally for several receptors including the epidermal growth factor receptor (EGFR), fibroblast growth factor receptor (FGFR), and tropomyosin receptor kinase A (TrkA) (52–55). It is believed that these electrostatic interactions serve to sequester phosphorylatable JM residues, rendering them inaccessible to the kinase domain, prior to ligand binding (53, 56). This effect is likely paired with the kinase domains also binding with the membrane, which has been shown *via* MD for EphA2, and experimentally for EGFR (56, 57).

We speculate that if ephrinA1 binds EphA2 in the ligand-independent dimeric conformation, the receptor would undergo rearrangements including TM rotation and opening of the crossing angle. Dimerization *via* the glycine zipper interface would not be promoted by PIP$_2$, but by interactions between other parts of the full-length protein that oligomerize such as the cysteine rich domains and the ligand binding domains, which interact through two different interfaces upon ligand binding (27, 39, 58). The glycine zipper TMD dimer may also be further stabilized by interactions with other proteins, which may contribute to the formation of large signaling clusters. For example, it is believed that interactions between SAM domains and dimers of SHIP2 may form large linear arrays (59, 60).

Our findings provide new insights that suggest that PIP$_2$, and maybe other phosphorylated inositol lipids, could directly act as a conditional ligand of EphA2, causing Akt-independent modulation of the ligand-independent conformation of the receptor. We are currently testing the hypothesis that the lipid environment specifically regulates EphA2 signaling in cells.

Experimental procedures

Liposome preparation

Lipids were purchased from Avanti Polar Lipids, Alabaster, AL. 14:1 PC (1,2-dimyristoleoyl-*sn*-glycero-3-phosphocholine), 22:1-PC (1,2-dierucoyl-*sn*-glycero-3-phosphocholine), PIP$_2$ (L-α-phosphatidylinositol-4,5-bisphosphate (Brain, Porcine)), 18:1 dansyl-PE (1,2-dioleoyl-*sn*-glycero-3-phosphoethanolamine-*N*-(5-dimethylamino-1-naphthalenesulfonyl)), POPC (1-palmitoyl-2-oleoyl-glycero-3-phosphocholine), biotin-PE (1-oleoyl-2-(12-biotinyl(aminododecanoyl))-*sn*-glycero-3-phosphoethanolamine), and PIP$_2$ Bodipy FL (Echelon Biosciences, Salt Lake City, UT) stocks were prepared in chloroform. Aliquots of lipids were dried under argon gas and then placed in a vacuum overnight. Unless otherwise noted, lipid films were resuspended with Buffer A: 19.3 mM HEPES (4-(2-hydroxyethyl)-1-piperazineethanesulfonic acid) buffer (pH 7.5), 1 mM EGTA (ethylene glycol-bis(β-aminoethyl ether)-*N*,*N*,*N*′,*N*′-tetraacetic acid), and 5 mM DTT (dithiothreitol). Large unilamellar vesicles (LUVs) were formed by extrusion with a Mini-Extruder (Avanti Polar Lipids, Alabaster, AL) through a 100 nm pore size membrane (Whatman, United Kingdom).

Peptide conjugation

The TMJM peptide was synthesized by F-moc chemistry by Thermo Fisher (Waltham, MA), and purity (>95%) was assessed by MALDI-TOF and HPLC. The cysteine residue of TMJM was conjugated to Alexa Fluor 488 (Molecular Probes, Eugene OR) or Cyanine5 (Cy5) (Fluoroprobes, Scottsdale AZ), using a C$_5$ maleimide moiety. The reaction was carried out by adding a molar excess (peptide:dye of 1:1.1 mol) of dye dissolved in 100 mM sodium phosphate pH 7.6 to a peptide stock in 2,2,2-trifluoroethanol (TFE). Unreacted dye was removed by HPLC, by injecting the TFE mixture onto a semipreparative Agilent Zorbax 300 SB-C18 column on an Agilent 1200 HPLC system (Santa Clara, CA). The gradient of water +0.05% trifluoroacetic acid (TFA) to acetonitrile +0.05% TFA was 30 min from 0% to 100% acetonitrile. The conjugated peptide eluted around 95% acetonitrile. The collected fractions from HPLC were frozen and lyophilized. The dry conjugated peptide was resuspended in hexafluoroisopropanol (HFIP).

MALDI-TOF

For matrix-assisted laser desorption ionization time of flight (MADLI-TOF) mass spectrometry measurements, peptide in solvent was mixed with a saturated solution of a-cyano-4-hydroxycinnamic acid (a-HCCA) in a mixture of 70% methanol and 0.05% trifluoroacetic acid. This solution was dried dropwise onto an MSP AnchorChip target plate (Bruker, Billerica, MA). Mass spectra were collected on a Bruker Microflex MALDI-TOF mass spectrometer, calibrated with the Bruker Peptide Calibration Standard II (Billerica, MA). Spectra were analyzed using FlexAnalysis software (Bruker, Billerica, MA).

Oriented circular dichroism

A stock of TMJM was prepared in TFE. Aliquots of 2.23×10^{-7} mol of 14:1 PC or 22:1 PC were dried under argon, then vacuum desiccated for at least 2 h. The appropriate amount of peptide stock (for a 50:1 or 300:1 lipid-to-peptide molar ratio) was added, dried with argon, and finally dried under vacuum for at least 2 h. The lipid–peptide film was resuspended with 400 µl TFE and 150 µl spread on each of two circular quartz slides (Hellma Analytics, Germany). To allow for even solvent evaporation, the slides were placed in a fume hood overnight and further dried under vacuum for at least 6 h to ensure complete evaporation of the TFE. The samples were hydrated under argon with 150 µl per slide of Buffer A overnight in 96% relative humidity, to obtain supported bilayers. Excess buffer was removed, and the hydrated slides were assembled in an OCD cell, with an inner cavity filled with saturated K_2SO_4 to keep the bilayers humidified. The OCD spectra were recorded on a Jasco J-815 spectropolarimeter at room temperature (19–21 °C). For each sample eight 45° rotations of the cell were averaged. Appropriate lipid backgrounds were subtracted in all cases. Sample tubes were washed with SDS and CD was performed to ensure that equivalent amounts of the peptide were recovered in each lipid when liposomes were resuspended. This was done assuming that the CD signal is directly proportional to protein concentration (61).

Tryptophan fluorescence

Thirteen millimeter glass culture tubes (Fisher Scientific) were cleaned with piranha (75% H_2SO_4, 25% H_2O_2) solution for 3 min, creating a hydrophilic surface to promote efficient removal of peptide. Appropriate amounts of 100% 22:1 PC/14:1 PC or 3 mol% PIP$_2$ and 97 mol% 22:1 PC/14:1 PC stocks were added to the cleaned tubes and dried under argon. Next, the lipids were dried under vacuum for at least 2 h before the appropriate amount of peptide stock was added to achieve a lipid-to-peptide molar ratio of 300:1 and subsequently dried under vacuum overnight. Films were resuspended in Buffer A for an initial peptide concentration of 4 µM and extruded. To maximize peptide recovery, resuspension was conducted in three stages. First, 50% of the buffer volume was added to the tube, then vortexed for 45 s. This buffer was removed, then the procedure was repeated twice with 25% of the final buffer volume. Equivalent lipid blanks were also prepared. To ensure that amounts of lipids between blanks and proteoliposomes were equal, ammonium molybdate phosphate assays were performed to quantify lipids (62). If necessary, lipid blank concentrations were appropriately adjusted. LUVs were then diluted to 300 µM lipid and 1 µM peptide ±5 mM CaCl$_2$ (where indicated). Samples were incubated for a minimum of 1 h at room temperature (19–21 °C) to allow calcium levels to equilibrate across the bilayer. Tryptophan fluorescence spectra were then collected on a Cary Eclipse Fluorescence Spectrophotometer (Agilent Scientific, Santa Clara, CA) using an excitation wavelength of 290 nm. Lipid blanks were subtracted in all cases.

Trp-DNS FRET

Lipids and peptide were dried in piranha-cleaned glass tubes as described above. Films were resuspended as described above in Buffer A for an initial peptide concentration of 4 µM. Equivalent lipid blanks were also prepared. Liposomes and proteoliposomes containing 0% and 10% dansyl-PE were mixed in appropriate ratios and subjected to seven rounds of freeze–thaw to achieve 0%, 0.25%, 0.5%, 1%, 2%, 3%, and 5% dansyl-PE, ± 1 µM peptide, and ±5 mM CaCl$_2$ final concentrations where indicated. Samples were incubated at room temperature (19–21 °C) for a minimum of 1 h to allow calcium levels to equilibrate. FRET experiments were conducted on a Cary Eclipse Fluorescence Spectrophotometer (Agilent Scientific, Santa Clara, CA) using an excitation wavelength of 290 nm. FRET efficiencies (E) were calculated with the following equation:

$$E = 1 - \frac{I_{DA}}{I_D}$$

Where I_{DA} is the intensity of the donor in the presence of acceptor and I_D is the intensity of the donor only.

Calcium influx assay

POPC vesicles were prepared by resuspending dried POPC with Buffer A, and 0.1 mM Indo-1 (1H-Indole-6-carboxylic acid, 2-[4-[bis-(carboxymethyl)amino]-3-[2-[2-(bis-carboxymethyl)amino-5-methylphenoxy]ethoxy]phenyl]-, pentapotassium salt). LUVs were formed *via* extrusion as described above. To separate encapsulated and free Indo-1, LUVs were subjected to size-exclusion chromatography on a Sephadex G25 PD-10 column (GE Life Sciences, Chicago, IL). The concentration of the encapsulated Indo-1 was estimated using fluorescence and known amounts of free Indo-1. Indo-1-containing LUVs were diluted to a final Indo-1 concentration of 0.05 µM in Buffer A and 5 mM CaCl$_2$ was added. Calcium influx was observed in a Cytation5 plate reader (BioTek, Winooski, VT) as a shift in fluorescence maximum from 485 nm to 405 nm. Calcium influx saturated after 5 min. Free dye with 5 mM CaCl$_2$ and encapsulated dye with 0.1% Triton X-100 were used as controls.

SMALP preparation

For photobleaching experiments, peptide and lipid films were prepared by drying down 22:1 PC or 14:1 PC + 3% biotin-PE ± 3% PIP$_2$ or 10% POPS from chloroform stocks. To this film TMJM conjugated with Alexa Fluor 488 in HFIP was added. For colocalization experiments, lipids and peptides were prepared the same way as in photobleaching experiments with PIP$_2$ Bodipy FL and TMJM conjugated to Cy5. The amount of lipid was kept constant while the amount of peptide was adjusted for the specified lipid-to-peptide ratio (300:1, 100:1 or 50:1). The films were dried under Ar gas, then vacuum-desiccated for at least 2 h. MLVs were then formed by resuspending in SMALP buffer (19.3 mM HEPES, 150 mM NaCl, 1 mM EGTA). MLVs were subjected to three rounds of

freeze–thaw at –80 °C and 42 °C to ensure even mixing of the lipid components. A stock solution of 1 to 9 mg/ml of SMA 2000H (Polyscope, Geleen, The Netherlands) was diluted to 0.3 mg/ml and added to MLVs for a SMA final concentration of 0.075 mg/ml and lipid concentration of 100 μM. The MLV/SMA solution was then incubated overnight with shaking to allow SMALP formation.

Single-molecule TIRF

Quartz microscope slides (G. Finkenbeiner Inc, Waltham MA) and coverslips were cleaned following the protocol of Chandradoss *et al.* 2014 (63). Clean slides and coverslips underwent animosalinization and PEGylating following a procedure previously described (64). In short, slides were incubated with a solution of 93% methanol, 4.5% acetic acid, and 2.5% 3-(triethoxysilyl)-propylamine (EMD Millipore Corp, Billerica, MA), rinsed with methanol and water, and finally dried under a stream of nitrogen (64). A solution of m-PEG-SVA and biotin-PEG-SVA (Laysan Bio Inc, Arab, AL) was made by dissolving 20% w/v m-PEG and 1.25% biotin-PEG in filtered 100 mM NaHCO₃ overnight. To assemble a flow chamber, slides were predrilled with holes and fitted with a coverslip using double-sided tape and sealed with vacuum grease. PEGylated slides were incubated for 10 min with 0.2 mg/ml streptavidin and then washed with SMALP buffer. SMALPs, containing a peptide concentration of 20 to 30 nM, were immobilized on the slides for 10 min and then rinsed to remove any nonspecific interactions. The rinse buffer was replaced with an oxygen-scavenging system; 2.5 mM PCA and 250 nM rPCO (recombinant Protocatechuate 3,4-Dioxygenase; Oriental Yeast Co, Tokyo Japan) in SMALP buffer with 2 mM Trolox (65). Slides were imaged under a custom-based TIRF microscope and the emission intensities were collected on CCD camera (Andor Technology) with 100 ms integration time. A custom-written software package (downloaded from https://physics.illinois.edu/cplc/software) was used to record movies and extract single-molecule traces using scripts written in IDL (Harris Geospatial Solutions, Inc) software (66). Single-molecule traces were assessed and analyzed using custom software written in Python and analyzed to determine the number of photobleaching steps. To prevent potential bias, the experimenter was blinded during analysis with a custom data-shuffling Python script.

SDS-PAGE

Lipid–peptide films were prepared for SDS PAGE as described above with unlabeled TMJM peptide at a lipid-to-peptide ratio of 300:1. Dried lipid–peptide films were resuspended in 19.3 mM HEPES, 1 mM EGTA and shaken at room temperature (19–21 °C) for 3 h to allow disulfide bond formation. To the MLVs, SDS buffer was added for a final SDS concentration of 150 mM. To this, sample buffer ± DTT was added. Samples were then boiled for 5 to 10 min to ensure complete disruption of liposomes. To ensure the stock of peptide did not contain disulfide-mediated dimers, a sample of the TMJM stock was also prepared without lipid. This sample was resuspended in buffer containing 150 mM SDS and loaded

with sample buffer without DTT. Samples were run on a 16% tricine gel and stained using a Pierce Silver Stain Kit (Thermo Scientific, Waltham MA). Bands were quantified in ImageJ using the Band Peak Quantification plugin.

Transmission electron microscopy

SMALPs were prepared as described above to a final lipid concentration of 1 mM. In total, 3% w/w SMA was added to both lipids before overnight equilibration. SMALPs of 14:1 PC were equilibrated with shaking at room temperature (19–21 °C) overnight, while 22:1 PC SMALPs were incubated at 60 °C for the same duration. SMALPS were imaged with negative staining TEM. Small aliquots of SMALPs were adsorbed on to glow discharged carbon-coated copper EM grids (Electron Microscopy Sciences, Hatfield, PA) for 120 s. Grids were washed twice with ddH₂O for 15 s before negative staining with UranyLess (Electron Microscopy Sciences, Hatfield, PA) for 45 s. Excess liquid was removed from the grid with filter paper between steps. Grids were air-dried prior to examination on a JEOL JEM 1400-Flash TEM (JEOL USA, Peabody, MA) operating at 80 kV. SMALPs were measured in ImageJ.

Statistical analysis

All statistical comparisons were made in IBM SPSS v25 software (Armonk, New York USA). Where only two means were compared, Student's *t*-tests were used. Where more than two means were compared, one-way analysis of variance (ANOVA) was conducted followed by post-hoc comparisons, with Tukey HSD tests where data were homoscedastic, and Dunnett's *t*-test where data were heteroscedastic. All *p*-values reflect an α = 0.05. Where no *p*-values are shown, the difference is not significant.

Data availability

All data are contained within the manuscript.

Abbreviations—The abbreviations used are: ALS, amyotrophic lateral sclerosis; ANOVA, analysis of variance; DTT, dithiothreitol; FRET, Förster resonance energy transfer; GZ, glycine zipper; HPLC, high-performance liquid chromatography; HR, heptad repeat; JM, juxtamembrane; MALDI-TOF, matrix-assisted laser desorption ionization time of flight; MD, molecular dynamics; OCD, oriented circular dichroism; PS, phosphatidylserine; RTK, receptor tyrosine kinase; SMALPs, styrene maleic acid lipid particles; TEM, transmission electron microscopy; TIRF, total internal reflection fluorescence; TM, transmembrane.

References

1. Boyd, A. W., Bartlett, P. F., and Lackmann, M. (2014) Therapeutic targeting of EPH receptors and their ligands. *Nat. Rev. Drug Discov.* **13**, 39–62
2. Pasquale, E. B. (2008) Eph-Ephrin bidirectional signaling in physiology and disease. *Cell* **133**, 38–52
3. Fu, A. K. Y., Hung, K.-W., Huang, H., Gu, S., Shen, Y., Cheng, E. Y. L., Ip, F. C. F., Huang, X., Fu, W.-Y., and Ip, N. Y. (2014) Blockade of EphA4 signaling ameliorates hippocampal synaptic dysfunctions in mouse models of Alzheimer's disease. *Proc. Natl. Acad. Sci. U. S. A.* **111**, 9959–9964
4. Vargas, L. M., Leal, N., Estrada, L. D., González, A., Serrano, F., Araya, K., Gysling, K., Inestrosa, N. C., Pasquale, E. B., and Alvarez, A. R. (2014) EphA4 activation of c-Abl mediates synaptic loss and LTP blockade caused by amyloid-β oligomers. *PLoS One* **9**, e92309
5. Van Hoecke, A., Schoonaert, L., Lemmens, R., Timmers, M., Staats, K. A., Laird, A. S., Peeters, E., Philips, T., Goris, A., Dubois, B., Andersen, P. M., Al-Chalabi, A., Thijs, V., Turnley, A. M., Van Vught, P. W., *et al.* (2012) EPHA4 is a disease modifier of amyotrophic lateral sclerosis in animal models and in humans. *Nat. Med.* **18**, 1418–1422
6. Zhao, J., Cooper, L. T., Boyd, A. W., and Bartlett, P. F. (2018) Decreased signalling of EphA4 improves functional performance and motor neuron survival in the SOD1G93A ALS mouse model. *Sci. Rep.* **8**, 11393
7. Risley, M., Garrod, D., Henkemeyer, M., and McLean, W. (2009) EphB2 and EphB3 forward signalling are required for palate development. *Mech. Dev.* **126**, 230–239
8. Fox, B. P., and Kandpal, R. P. (2004) Invasiveness of breast carcinoma cells and transcript profile: Eph receptors and ephrin ligands as molecular markers of potential diagnostic and prognostic application. *Biochem. Biophys. Res. Commun.* **318**, 882–892
9. Lin, Y. G., Han, L. Y., Kamat, A. A., Merritt, W. M., Landen, C. N., Deavers, M. T., Fletcher, M. S., Urbauer, D. L., Kinch, M. S., and Sood, A. K. (2007) EphA2 overexpression is associated with angiogenesis in ovarian cancer. *Cancer* **109**, 332–340
10. Zeng, G., Hu, Z., Kinch, M. S., Pan, C. X., Flockhart, D. A., Kao, C., Gardner, T. A., Zhang, S., Li, L., Baldridge, L. A., Koch, M. O., Ulbright, T. M., Eble, J. N., and Cheng, L. (2003) High-level expression of EphA2 receptor tyrosine kinase in prostatic intraepithelial neoplasia. *Am. J. Pathol.* **163**, 2271–2276
11. Miyazaki, T., Kato, H., Fukuchi, M., Nakajima, M., and Kuwano, H. (2003) EphA2 overexpression correlates with poor prognosis in esophageal squamous cell carcinoma. *Int. J. Cancer* **103**, 657–663
12. Kinch, M. S., Moore, M. B., and Harpole, D. H. (2003) Predictive value of the EphA2 receptor tyrosine kinase in lung cancer recurrence and survival. *Clin. Cancer Res.* **9**, 613–618
13. Thaker, P. H., Deavers, M., Celestino, J., Thornton, A., Fletcher, M. S., Landen, C. N., Kinch, M. S., Kiener, P. A., and Sood, A. K. (2004) EphA2 expression is associated with aggressive features in ovarian carcinoma. *Clin. Cancer Res.* **10**, 5145–5150
14. Duxbury, M. S., Ito, H., Zinner, M. J., Ashley, S. W., and Whang, E. E. (2004) EphA2: a determinant of malignant cellular behavior and a potential therapeutic target in pancreatic adenocarcinoma. *Oncogene* **23**, 1448–1456
15. Chen, J., Schaller, S., Jardetzky, T. S., and Longnecker, R. (2020) EBV gH/gL and KSHV gH/gL bind to different sites on EphA2 to trigger fusion. *J. Virol.* **94**, e01454-20
16. Hahn, A. S., Kaufmann, J. K., Wies, E., Naschberger, E., Panteleev-Ivlev, J., Schmidt, K., Holzer, A., Schmidt, M., Chen, J., König, S., Ensser, A., Myoung, J., Brockmeyer, N. H., Stürzl, M., Fleckenstein, B., *et al.* (2012) The ephrin receptor tyrosine kinase A2 is a cellular receptor for Kaposi's sarcoma-associated herpesvirus. *Nat. Med.* **18**, 961–966
17. Pasquale, E. B. (2010) Eph receptors and ephrins in cancer: bidirectional signalling and beyond. *Nat. Rev. Cancer* **10**, 165–180
18. Miao, H., Li, D. Q., Mukherjee, A., Guo, H., Petty, A., Cutter, J., Basilion, J. P., Sedor, J., Wu, J., Danielpour, D., Sloan, A. E., Cohen, M. L., and Wang, B. (2009) EphA2 mediates ligand-dependent inhibition and ligand-independent promotion of cell migration and invasion via a reciprocal regulatory loop with Akt. *Cancer Cell* **16**, 9–20
19. Miao, H., Burnett, E., Kinch, M., Simon, E., and Wang, B. (2000) Activation of EphA2 kinase suppresses integrin function and causes focal-adhesion-kinase dephosphorylation. *Nat. Cell Biol.* **2**, 62–69
20. Paraiso, K. H. T., Das Thakur, M., Fang, B., Koomen, J. M., Fedorenko, I. V., John, J. K., Tsao, H., Flaherty, K. T., Sondak, V. K., Messina, J. L., Pasquale, E. B., Villagra, A., Rao, U. N., Kirkwood, J. M., Meier, F., *et al.* (2015) Ligand-independent EPHA2 signaling drives the adoption of a targeted therapy-mediated metastatic melanoma phenotype. *Cancer Discov.* **5**, 264–273
21. Zhou, Y., Yamada, N., Tanaka, T., Hori, T., Yokoyama, S., Hayakawa, Y., Yano, S., Fukuoka, J., Koizumi, K., Saiki, I., and Sakurai, H. (2015) Crucial roles of RSK in cell motility by catalysing serine phosphorylation of EphA2. *Nat. Commun.* **6**, 1–12
22. Barquilla, A., Lamberto, I., Noberini, R., Heynen-Genel, S., Brill, L. M., and Pasquale, E. B. (2016) Protein kinase A can block EphA2 receptor-mediated cell repulsion by increasing EphA2 S897 phosphorylation. *Mol. Biol. Cell* **27**, 2757–2770
23. Hafner, C., Schmitz, G., Meyer, S., Bataille, F., Hau, P., Langmann, T., Dietmaier, W., Landthaler, M., and Vogt, T. (2004) Differential gene expression of Eph receptors and ephrins in benign human tissues and cancers. *Clin. Chem.* **50**, 490–499
24. Macrae, M., Neve, R. M., Rodriguez-Viciana, P., Haqq, C., Yeh, J., Chen, C., Gray, J. W., and McCormick, F. (2005) A conditional feedback loop regulates Ras activity through EphA2. *Cancer Cell* **8**, 111–118
25. Wykosky, J., and Debinski, W. (2008) The EphA2 receptor and EphrinA1 ligand in solid tumors: function and therapeutic targeting. *Mol. Cancer Res.* **6**, 1795–1806
26. Singh, D. R., Ahmed, F., King, C., Gupta, N., Salotto, M., Pasquale, E. B., and Hristova, K. (2015) EphA2 receptor unliganded dimers suppress EphA2 pro-tumorigenic signaling. *J. Biol. Chem.* **290**, 27271–27279
27. Himanen, J. P., Yermekbayeva, L., Janes, P. W., Walker, J. R., Xu, K., Atapattu, L., Rajashankar, K. R., Mensinga, A., Lackmann, M., Nikolov, D. B., and Dhe-Paganon, S. (2010) Architecture of Eph receptor clusters. *Proc. Natl. Acad. Sci. U. S. A.* **107**, 10860–10865
28. Bocharov, E. V., Mayzel, M. L., Volynsky, P. E., Mineev, K. S., Tkach, E. N., Ermolyuk, Y. S., Schulga, A. A., Efremov, R. G., and Arseniev, A. S. (2010) Left-handed dimer of EphA2 transmembrane domain: helix packing diversity among receptor tyrosine kinases. *Biophys. J.* **98**, 881–889
29. Sharonov, G. V., Bocharov, E. V., Kolosov, P. M., Astapova, M. V., Arseniev, A. S., and Feofanov, A. V. (2014) Point mutations in dimerization motifs of the transmembrane domain stabilize active or inactive state of the EphA2 receptor tyrosine kinase. *J. Biol. Chem.* **289**, 14955–14964
30. Hedger, G., Sansom, M. S. P., and Koldsø, H. (2015) The juxtamembrane regions of human receptor tyrosine kinases exhibit conserved interaction sites with anionic lipids. *Sci. Rep.* **5**, 1–10
31. Kučerka, N., Gallová, J., Uhríková, D., Balgavý, P., Bulacu, M., Marrink, S. J., and Katsaras, J. (2009) Areas of monounsaturated diacylphosphatidylcholines. *Biophys. J.* **97**, 1926–1932
32. Nyholm, T. K. M., Özdirekcan, S., and Antoinette Killian, J. (2007) How protein transmembrane segments sense the lipid environment. *Biochemistry* **46**, 1457–1465
33. Wu, Y., Huang, H. W., and Olah, G. A. (1990) Method of oriented circular dichroism. *Biophys. J.* **57**, 797–806
34. Burck, J., Wadhwani, P., Fangha, S., and Ulrich, A. S. (2016) Oriented circular dichroism: a method to characterize membrane-active peptides in oriented lipid bilayers. *Acc. Chem. Res.* **49**, 184–192

35. Ulmschneider, M. B., Ulmschneider, J. P., Schiller, N., Wallace, B. A., Von Heijne, G., and White, S. H. (2014) Spontaneous transmembrane helix insertion thermodynamically mimics translocon-guided insertion. *Nat. Commun.* **5**, 4863

36. Postis, V., Rawson, S., Mitchell, J. K., Lee, S. C., Parslow, R. A., Dafforn, T. R., Baldwin, S. A., and Muench, S. P. (2015) The use of SMALPs as a novel membrane protein scaffold for structure study by negative stain electron microscopy. *Biochim. Biophys. Acta* **1848**, 496–501

37. Knowles, T. J., Finka, R., Smith, C., Lin, Y. P., Dafforn, T., and Overduin, M. (2009) Membrane proteins solubilized intact in lipid containing nanoparticles bounded by styrene maleic acid copolymer. *J. Am. Chem. Soc.* **131**, 7484–7485

38. Ladokhin, A. S., Jayasinghe, S., and White, S. H. (2000) How to measure and analyze tryptophan fluorescence in membranes properly , and why bother ? *Anal. Biochem.* **245**, 235–245

39. Singh, D. R., Kanvinde, P., King, C., Pasquale, E. B., and Hristova, K. (2018) The EphA2 receptor is activated through induction of distinct, ligand-dependent oligomeric structures. *Commun. Biol.* **1**, 15

40. Gulamhussein, A. A., Meah, D., Soja, D. D., Fenner, S., Saidani, Z., Akram, A., Lallie, S., Mathews, A., Painter, C., Liddar, M. K., Mohammed, Z., Chiu, L. K., Sumar, S. S., Healy, H., Hussain, N., *et al.* (2019) Examining the stability of membrane proteins within SMALPs. *Eur. Polym. J.* **112**, 120–125

41. Toner, M., Vaio, G., McLaughlin, A., and McLaughlin, S. (1988) Adsorption of cations to phosphatidylinositol 4,5-bisphosphate. *Biochemistry* **27**, 7435–7443

42. Van Meer, G., Voelker, D. R., and Feigenson, G. W. (2008) Membrane lipids: where they are and how they behave. *Nat. Rev. Mol. Cell Biol.* **9**, 112–124

43. Alves, D. S., Westerfield, J. M., Shi, X., Nguyen, V. P., Stefanski, K. M., Booth, K. R., Kim, S., Morrell-Falvey, J., Wang, B. C., Abel, S. M., Smith, A. W., and Barrera, F. N. (2018) A novel pH-dependent membrane peptide that binds to EphA2 and inhibits cell migration. *Elife* **7**, 1–22

44. Nguyen, V. P., Dixson, A. C., and Barrera, F. N. (2019) Article the effect of phosphatidylserine on a pH-responsive peptide is defined by its non-inserting end. *Biophys. J.* **117**, 659–667

45. Chavent, M., Karia, D., Kalli, A. C., Domański, J., Duncan, A. L., Hedger, G., Stansfeld, P. J., Seiradake, E., Jones, E. Y., and Sansom, M. S. P. (2018) Interactions of the EphA2 kinase domain with PIPs in membranes: implications for receptor function. *Structure* **26**, 1025–1034.e2

46. Chen, Y., and Barkley, M. D. (1998) Toward understanding tryptophan fluorescence in proteins. *Biochemistry* **37**, 9976–9982

47. Vivian, J. T., and Callis, P. R. (2001) Mechanisms of tryptophan fluorescence shifts in proteins. *Biophys. J.* **80**, 2093–2109

48. Brooks, A. J., Dai, W., Mara, M. L. O., Abankwa, D., Chhabra, Y., Pelekanos, R. A., Gardon, O., Tunny, K. A., Blucher, K. M., Morton, C. J., Parker, M. W., Sierecki, E., Gambin, Y., Gomez, G. A., Alexandrov, K., *et al.* (2014) Mechanism of activation of protein kinase JAK2 by the growth hormone receptor. *Science* **344**, 1249783

49. Slochower, D. R., Huwe, P. J., Radhakrishnan, R., and Janmey, P. A. (2013) Quantum and all-atom molecular dynamics simulations of protonation and divalent ion binding to phosphatidylinositol 4,5-bisphosphate (PIP2). *J. Phys. Chem. B.* **117**, 8322–8329

50. Boettcher, J. M., Davis-Harrison, R. L., Clay, M. C., Nieuwkoop, A. J., Ohkubo, Y. Z., Tajkhorshid, E., Morrissey, J. H., and Rienstra, C. M. (2011) Atomic view of calcium-induced clustering of phosphatidylserine in mixed lipid bilayers. *Biochemistry* **50**, 2264–2273

51. Shi, X., Hapiak, V., Zheng, J., Muller-Greven, J., Bowman, D., Lingerak, R., Buck, M., Wang, B. C., and Smith, A. W. (2017) A role of the SAM domain in EphA2 receptor activation. *Sci. Rep.* **7**, 1–12

52. Michailidis, I. E., Rusinova, R., Georgakopoulos, A., Chen, Y., Iyengar, R., Robakis, N. K., Logothetis, D. E., and Baki, L. (2011) Phosphatidylinositol-4,5-bisphosphate regulates epidermal growth factor receptor activation. *Pflugers Arch. Eur. J. Physiol.* **461**, 387–397

53. Tamagaki, H., Furukawa, Y., Yamaguchi, R., Hojo, H., Aimoto, S., Smith, S. O., and Sato, T. (2014) Coupling of transmembrane helix orientation to membrane release of the juxtamembrane region in FGFR3. *Biochemistry* **53**, 5000–5007

54. Wang, Z., Fan, H., Hu, X., Khamo, J., Diao, J., Zhang, K., and Pogorelov, T. V. (2019) Coaction of electrostatic an hyrophobic interactions: dynamic constraints on disorere TrkA juxtamembrane domain. *J. Phys. Chem. B.* **123**, 10709–10717

55. Westerfield, J. M., and Barrera, F. N. (2020) Membrane receptor activation mechanisms and transmembrane peptide tools to elucidate them. *J. Biol. Chem.* **295**, 1792–1814

56. McLaughlin, S., Smith, S. O., Hayman, M. J., and Murray, D. (2005) An electrostatic engine model for autoinhibition and activation of the epidermal growth factor receptor (EGFR/ErbB) family. *J. Gen. Physiol.* **126**, 41–53

57. Chavent, M., Seiradake, E., Jones, E. Y., and Sansom, M. S. P. (2016) Structures of the EphA2 receptor at the membrane: role of lipid interactions. *Structure* **24**, 337–347

58. Seiradake, E., Harlos, K., Sutton, G., Aricescu, A. R., and Jones, E. Y. (2010) An extracellular steric seeding mechanism for Eph-ephrin signaling platform assembly. *Nat. Struct. Mol. Biol.* **17**, 398–402

59. Borthakur, S., Lee, H. J., Kim, S. J., Wang, B. C., and Buck, M. (2014) Binding and function of phosphotyrosines of the ephrin A2 (EphA2) receptor using synthetic sterile α motif (SAM) domains. *J. Biol. Chem.* **289**, 19694–19703

60. Lee, H. J., Hota, P. K., Chugha, P., Guo, H., Miao, H., Zhang, L., Kim, S. J., Stetzik, L., Wang, B. C., and Buck, M. (2012) NMR structure of a heterodimeric SAM:SAM complex: characterization and manipulation of EphA2 binding reveal new cellular functions of SHIP2. *Structure* **20**, 41–55

61. Kelly, S. M., Jess, T. J., and Price, N. C. (2005) How to study proteins by circular dichroism. *Biochim. Biophys. Acta.* **1751**, 119–139

62. Fiske, C. H., and Subbarow, Y. (1925) The colorimetric determination of phosphorus. *J. Biol. Chem.* **66**, 375–400

63. Chandradoss, S. D., Haagsma, A. C., Lee, Y. K., Hwang, J. H., Nam, J. M., and Joo, C. (2014) Surface passivation for single-molecule protein studies. *J. Vis. Exp.* https://doi.org/10.3791/50549

64. Lamichhane, R., Solem, A., Black, W., and Rueda, D. (2010) Single-molecule FRET of protein-nucleic acid and protein-protein complexes: surface passivation and immobilization. *Methods* **52**, 192–200

65. Aitken, C. E., Marshall, R. A., and Puglisi, J. D. (2008) An oxygen scavenging system for improvement of dye stability in single-molecule fluorescence experiments. *Biophys. J.* **94**, 1826–1835

66. Tinnefeld, P. (2011) Pull-down for single molecules. *Nature* **473**, 461–462

ASBMB